Electronic Supplementary Material (ESI) for Journal of Materials Chemistry A.
This journal is © The Royal Society of Chemistry 2020

Hardwood versus softwood Kraft lignin – precursor-product relationships in the manufacture of porous carbon nanofibers for supercapacitors

Philipp Schlee[a], Omid Hosseinaei[b], Christopher A. O' Keefe[c], María José Mostazo-Lopéz[d], Diego Cazorla-Amorós[d], Servann Herou[a], Per Tomani[b], Clare P. Grey[c], Maria-Magdalena Titirici[a]*

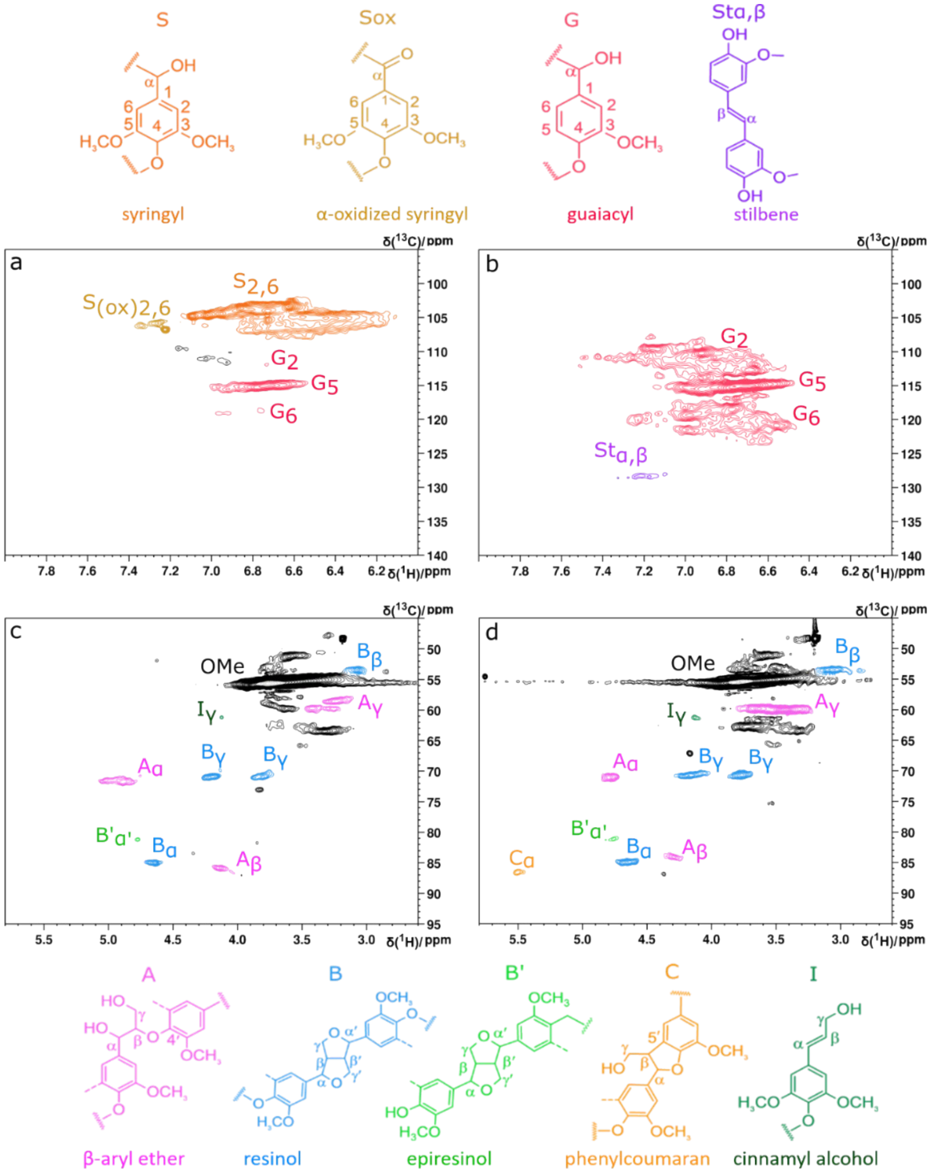

Supplementary information

Figure S. 1 Aromatic (top) and side-chain (bottom) regions of the ^{1}H-^{13}C HSQC NMR spectra of HKL (a and c) and SKL (b and d) together with the signal assignments.

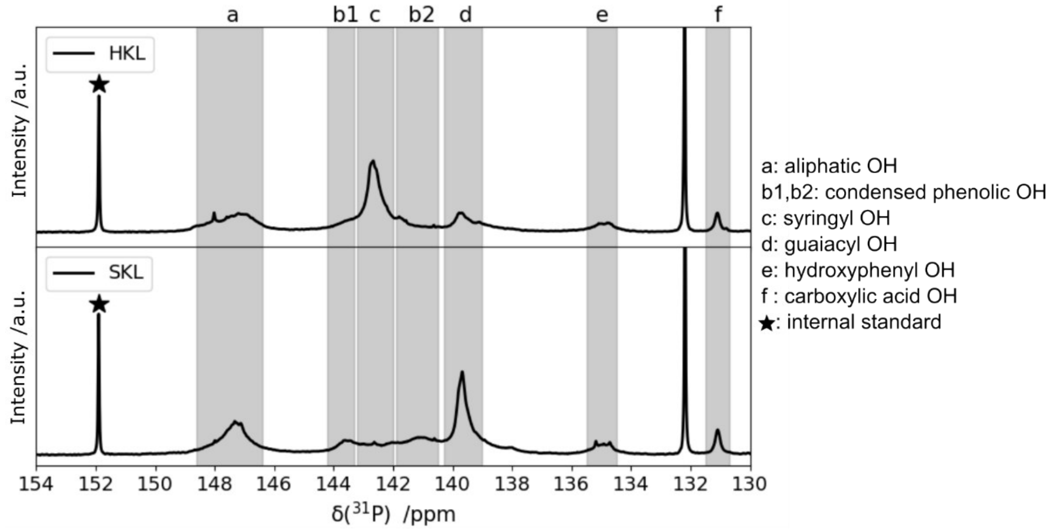

Figure S. 2 ^{31}P spectra of HKL and SKL with signal assignments. The star indicates the signal of the internal standard (N-hydroxy-5-norbornene-2,3-dicarboxylic acid imide).

Table S. 1 Experimentally optimized ^{1}H-^{13}C CP/MAS NMR acquisition parameters.

Sample	^{1}H T_1 (s)	Recycle delay (s)	Contact time (µs)
as-spun -SKL	0.366	1.830	500
S190-SKL	0.683	3.415	500
S250-SKL	0.239	1.197	1000
S310-SKL	0.101	0.505	250
S340-SKL	0.071	0.353	450
as-spun -HKL	0.390	1.950	500
S190_HKL	0.418	2.091	700
S250_HKL	0.213	1.065	1000
S310_HKL	0.052	0.209	250
S340_HKL	0.029	0.143	300

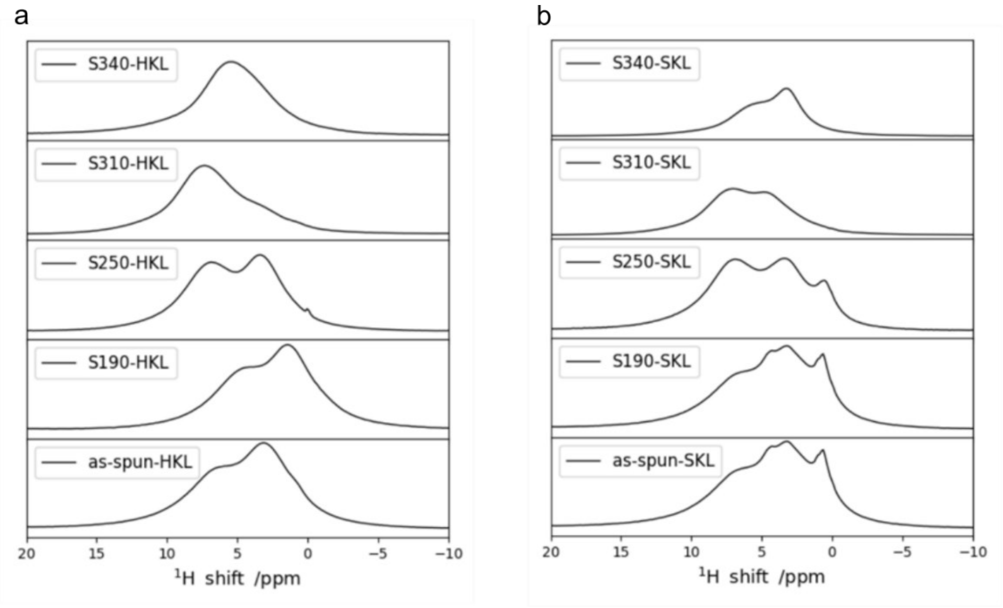

Figure S. 3 ^{1}H MAS NMR spectra of HKL (a) and SKL (b).

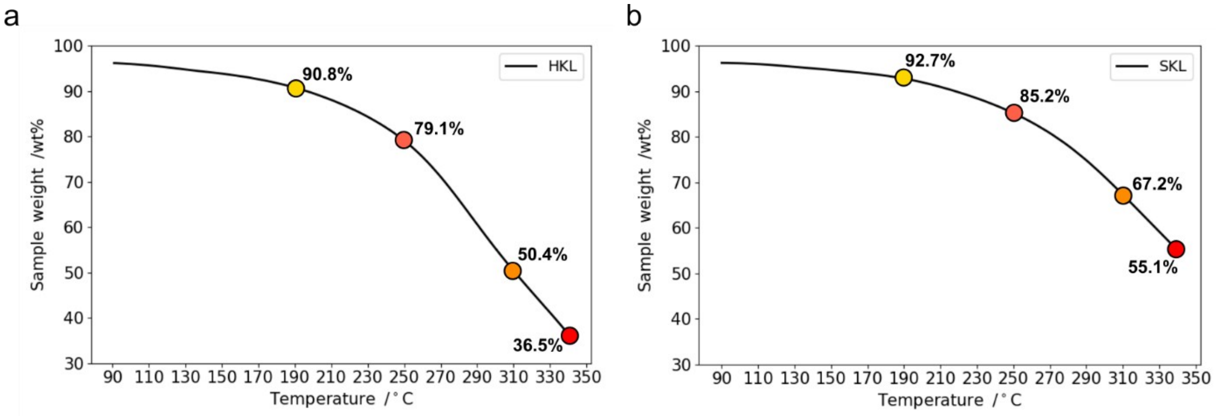

Figure S. 4 Weight loss traces of HKL (a) and SKL (b) from TGA

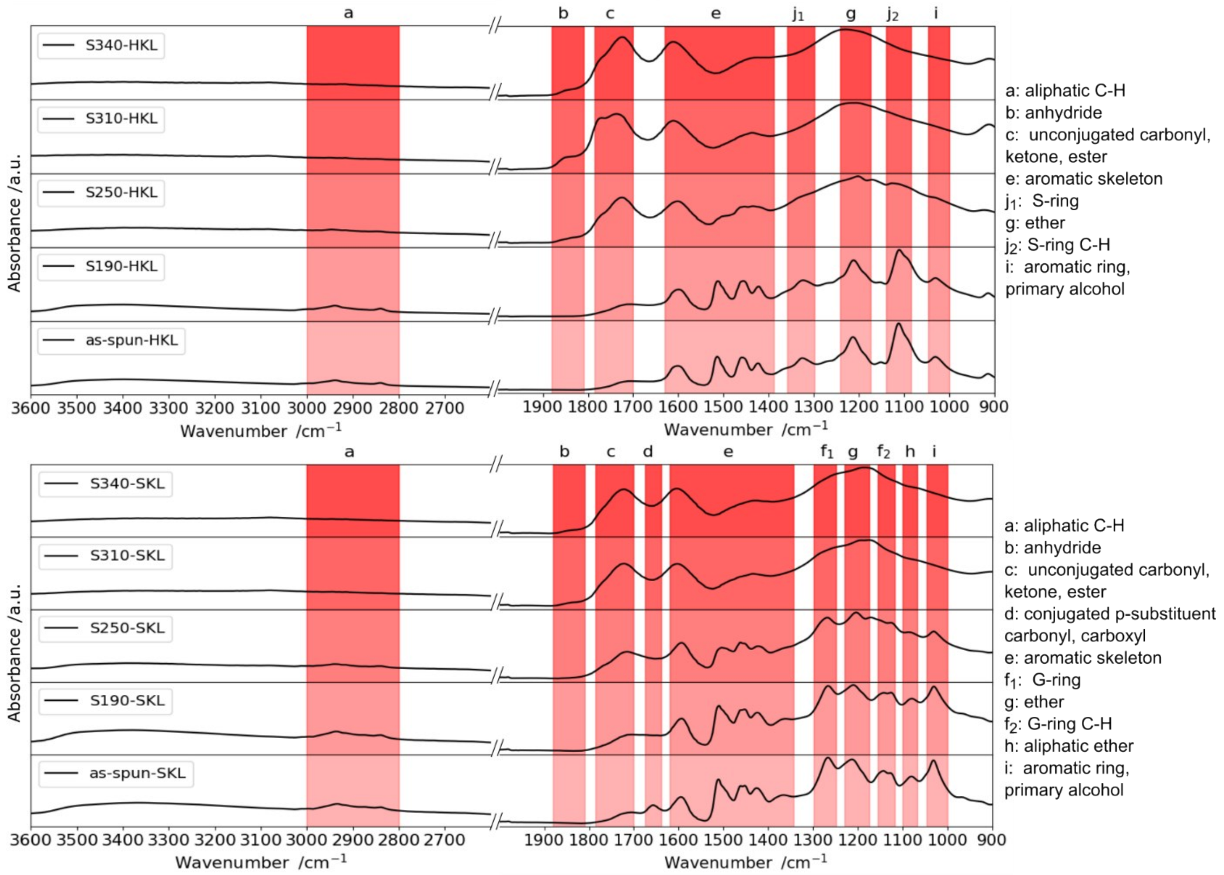

Figure S. 5 FTIR spectra of as-spun and stabilized samples derived from HKL (top) and SKL (bottom).

Complementary to ^{13}C CP/MAS NMR spectroscopy, Fourier transform infrared (FTIR) spectroscopy was carried out for the as-spun and stabilized samples. The spectra of HKL and SKL are shown in Figure S. 5. The two weak bands between 3000 and 2800 cm^{-1} (zone a) assigned to aliphatic C-H bonds and to the C-H stretching of aromatic methoxy groups decrease with increasing stabilization temperature.[1] The band disappears completely at a stabilization temperature of 250 °C for HKL. However, SKL still shows very weak residual intensity of this band. At a stabilization temperature of 310 °C, the band also disappears in the spectrum of SKL.

In the region between 1710 and 1880 cm^{-1} (zone b and c) corresponding to anhydride linkages (1880 – 1810 cm^{-1}), unconjugated carbonyl groups (1700 – 1750 cm^{-1}), aliphatic esters (1722 cm^{-}

^{1}) and aromatic esters (1770 cm^{-1}), an increase in intensities with increasing stabilization temperature can be observed for both lignins.[1,2] However, at a low stabilization temperature of 190 °C, the change in intensity of these bands are negligible, which indicates that no substantial crosslinking reactions took place.

This is consistent with the ^{13}C CP/MAS NMR and TG-MS data. However, a slight decrease in intensity in the region of conjugated carbonyl groups (1675 – 1639 cm^{-1}, zone d) and a concomitant increase in intensity of the unconjugated carbonyl, ketones, and ester bands (1700 – 1785 cm^{-1}, zone c) can be observed for SKL. Upon stabilization at 250 °C, a new, weak band appears at 1850 cm^{-1} in the spectrum of HKL which corresponds to the formation of anhydride linkages. This band is not yet observed for SKL at this temperature. However, the intensity of the band between 1700 – 1785 cm^{-1} (zone c) increases for both lignins indicating oxidation of the side chain. Upon stabilization at 310 °C, both lignins show an increase in intensity of the band characteristic of anhydride linkages (1850 cm^{-1}) and unconjugated carbonyl, ketones, and ester groups between 1700 and 1785 cm^{-1} (zone c). At a stabilization temperature of 340 °C, the intensity of the band assigned to anhydride linkages (1850 cm^{-1}) decreases slightly for HKL and remains unchanged in the spectrum of SKL. This is in line with the TG-MS data which showed that CO_2 is the main product arising from HKL and SKL indicating the cleavage of more stable C-C bonds (degradation) rather than formation of new bonds (crosslinking). In addition, the weight loss during stabilization shown in Figure S. 4 reveals substantial weight losses at 340 °C which supports the conclusion of excessive stabilization (polymer degradation). The FTIR spectra of SKL, however, remain unchanged between 310 and 340 °C, which underpins its higher thermal stability and recalcitrance due to the higher number of C-C linkages, lower amount of methoxy groups and higher carbon content resulting in a higher T_g. The four aromatic skeleton vibrational modes between 1343 and 1619 cm^{-1} (zone e) gradually disappear in both lignins with increasing temperature, whereas the one at around 1600 cm^{-1} (aromatic ring stretch) gradually increases in intensity, indicating a higher degree of condensation (C-C bonds).[3] The lignin specific bands: G-ring (zone f_1, f_2) for SKL and S-ring (zone j_1, j_2) for HKL merge with increasing temperature which can be explained by the loss of the substituents (methoxy and hydroxyl groups).[3] Additionally, the band indicative of ether bonds in the region of 1230 – 1174 cm^{-1}, the band characteristic of aliphatic ethers (zone h) only observed in SKL and the band of primary alcohol of the aromatic units (zone i) all merge into one very broad absorption band upon rising stabilization temperature. This occurs at a temperature of 250 °C for HKL. In SKL, it is observed at 310 °C due to its lower reactivity.

Table S. 2 Average diameters of fibers and density of the carbonized fiber mats.

	HKL		SKL	
Stabilization Temperature /°C	Average fiber diameter /nm	Density (carbonized) /g/cm^3	Average fiber diameter /nm	Density (carbonized) /g/cm^3
190	n.d.	n.d.	477± 109	0.19
250	460 ± 115	0.17	471± 106	0.15
310	371 ± 89	0.13	470± 106	0.11
340	280 ± 69	0.13	469± 105	0.11

Table S. 3 Overview over data obtained from the N_2 and CO_2 gas sorption experiments.

	N_2 sorption					CO_2 adsorption			
Sample	BET* SSA/ $m^2\ g^{-1}$	DFT SSA/ $m^2\ g^{-1}$	Total pore vol./ $cm^3\ g^{-1}$	Pore vol. <2nm/ $cm^3\ g^{-1}$	Pore vol. fraction <2nm/%	DFT SSA/ $m^2\ g^{-1}$	Pore** vol./ $cm^3\ g^{-1}$	Pore vol. <0.8nm/ $cm^3\ g^{-1}$	Pore vol. fraction <0.8nm/%
S250-HKL	588	954	0.24	0.21	87.5	1225	0.39	0.24	61.5
S310-HKL	845	1363	0.41	0.28	68.3	1383	0.44	0.27	61.4
S340-HKL	918	1552	0.35	0.33	94.3	1323	0.41	0.25	61.0
S190-SKL	528	804	0.34	0.15	44.1	982	0.29	0.19	65.5
S250-SKL	591	913	0.29	0.20	69.0	1131	0.35	0.22	63.0
S310-SKL	602	1034	0.31	0.20	64.5	1174	0.35	0.23	64.0
S340-SKL	668	1189	0.31	0.23	74.2	1267	0.40	0.24	60.0

*rel. pressure range used: 0.005-0.034.

**pore volume of pores with diameters in the range of 0.30 - 1.48 nm.

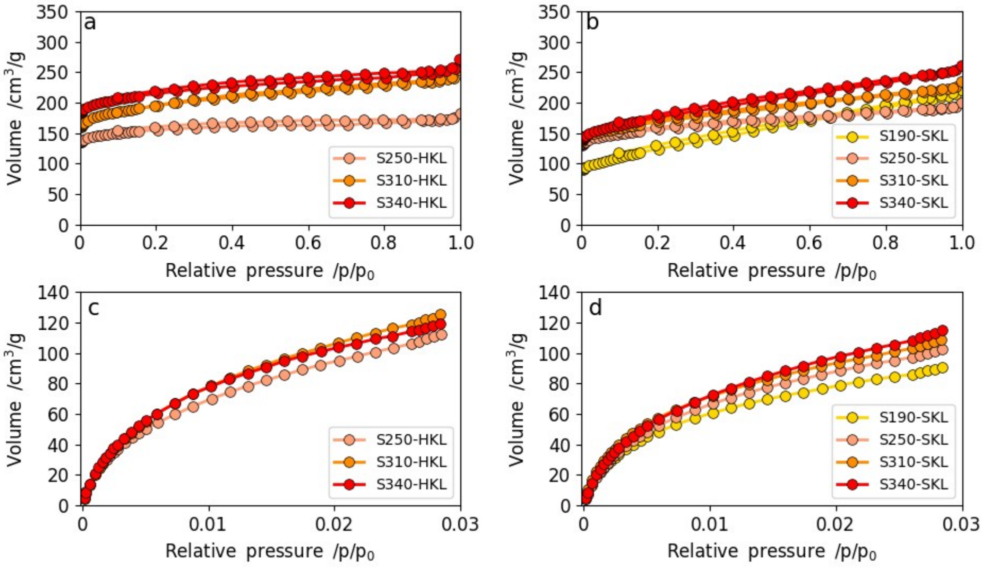

Figure S. 6 N_2 sorption isotherms of LCNFs derived from HKL (a) and SKL (b) and CO_2 adsorption isotherms of LCNFs derived from HKL (c) and SKL (d).

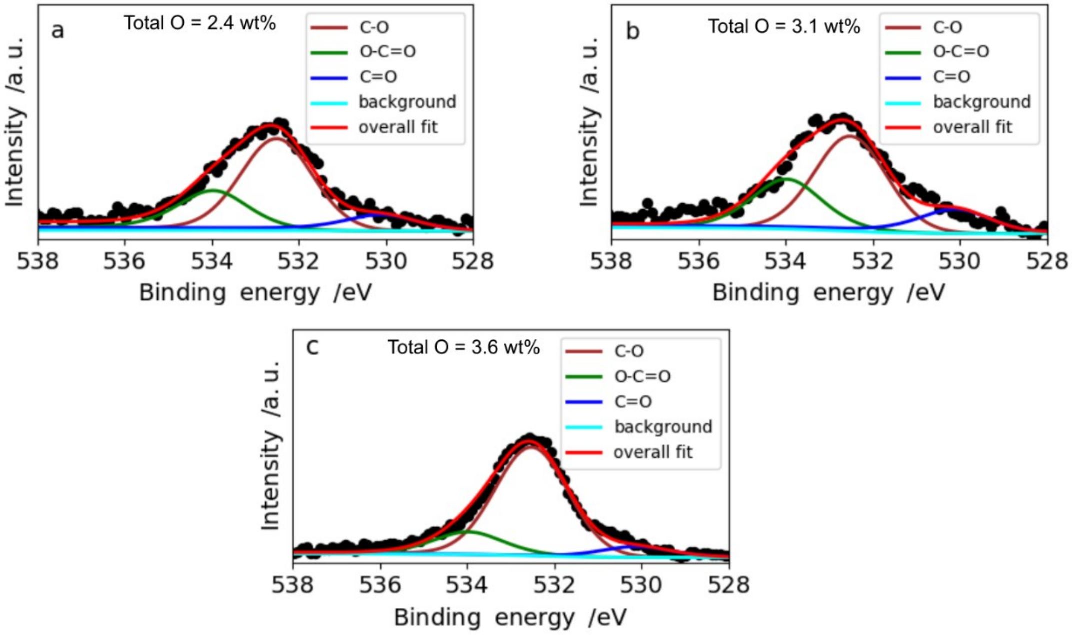

Figure S. 7 XPS O1s narrow scan spectra of LCNF derived from HKL.

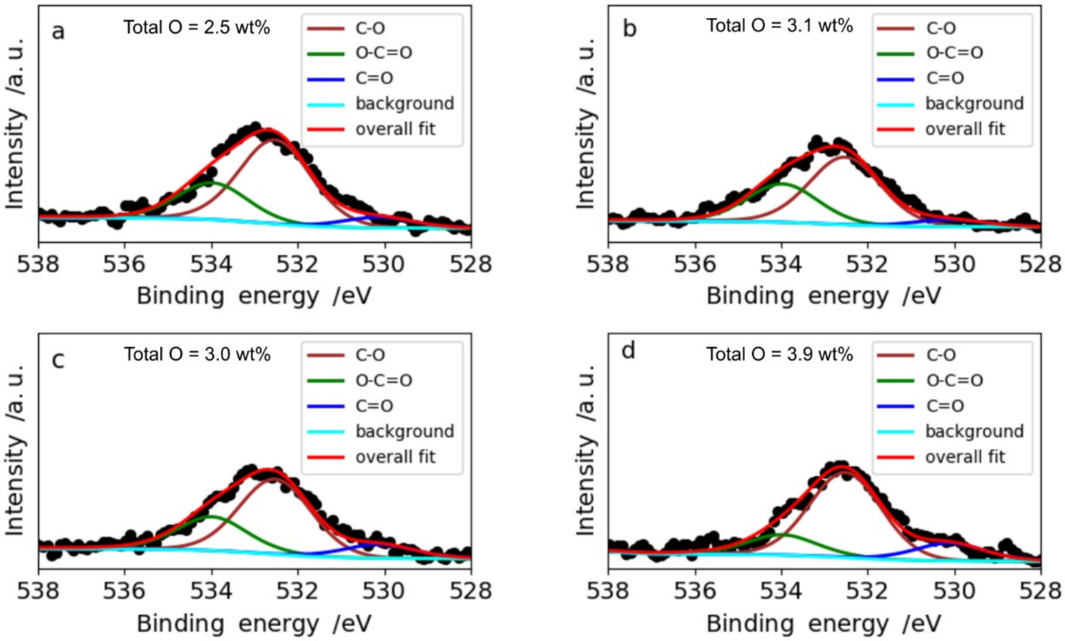

Figure S. 8 XPS O1s narrow scan spectra of LCNF derived from SKL.

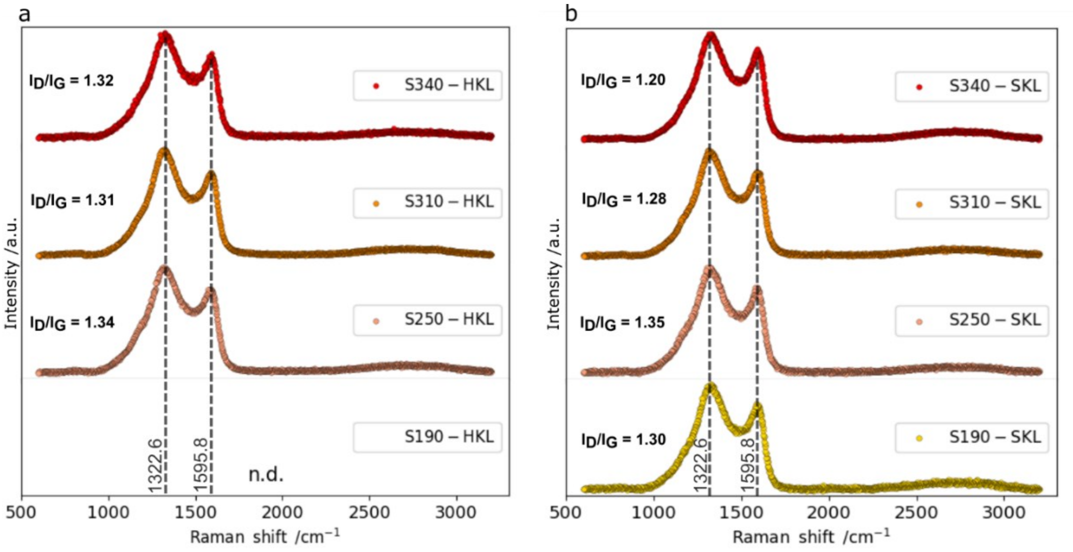

Figure S. 9 Raman spectra of the carbon nanofibers derived from HKL (a) and SKL (b) stabilized at different temperatures.

The Raman spectra of the LCNFs stabilized at various temperatures are shown in Figure S. 9. Both the D (1322.6 cm^{-1}) and G band (1595.8 cm^{-1}) characteristic of disordered carbons can be observed for all samples.[4] The 2D band (~2700 cm^{-1}) indicating graphene layers (2D ordering) are hardly discernible.[4] Moreover, the spectra of the LCNFs derived from HKL and SKL show hardly any changes in terms of position or intensity with increasing stabilization temperatures, which was reported in the literature previously.[5] Hence, the structure of the resulting CNFs is disordered and does not change substantially with increasing stabilization temperature. This is also indicated by the I(D)/I(G) ratios given in Figure S. 9, where the intensities are determined by the peak heights of the D and G bands. The values range from 1.20 to 1.35 which is only a slight variation. Therefore, the overall disordered carbon structure does not change upon increase of the stabilization temperature.

The cyclic voltammograms measured at 10 mV/s and 500 mV/s are shown in Figure S. 10 for HKL and in Figure S. 11 for SKL-derived LCNFs. S250-HKL shows the rectangular voltammograms characteristic of electric double layer supercapacitors at slow and high scan rate. Similarly, the cyclic voltammograms of S310-HKL and S340-HKL have a rectangular shape, but they also show signs of an irreversible process close to the maximum voltage of 1.2 V at low scan rate (10 mV/s) related to electrolyte decomposition. This process is not present at high scan rates, which implies it is rate dependent. However, for slow rates the cut-off voltage will need to be 1 V in practical supercapacitors. At 500 mV/s, it is also apparent that the rate capability of S310-HKL and S340-HKL is higher than for S250-HKL as the cyclic voltammogram of S250-HKL has curved edges at 500 mV/s, whereas S310-HKL and S340-HKL keep the rectangular shape. This can be related to the more open pore structure created by stabilization at higher temperatures involving both crosslinking and degradation reactions.

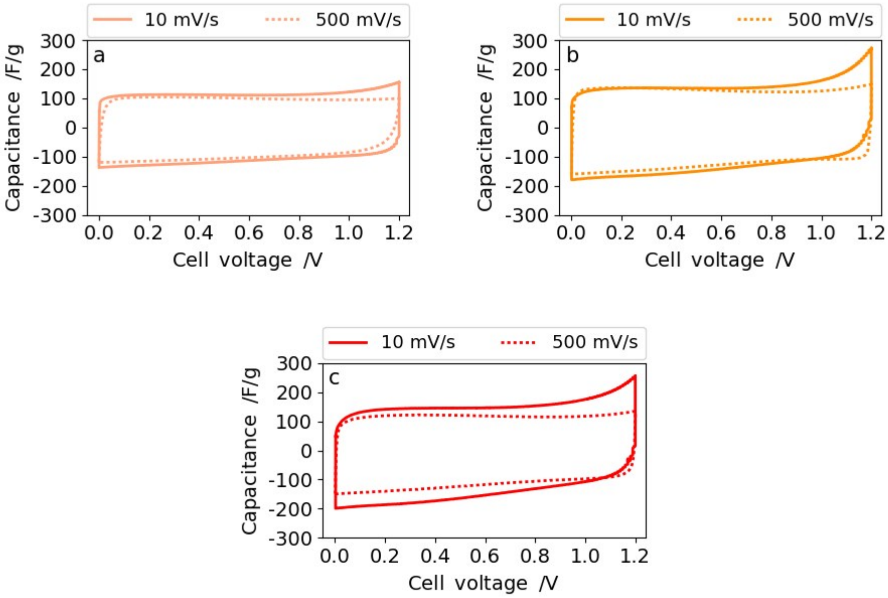

Figure S. 10 Cyclic voltammograms of S250-HKL (a), S310-HKL (b), S340-HKL (c) at 10 and 500 mV/s.

S190-SKL and S250-SKL show both lower rate capability (non-rectangular shape of voltammograms) and lower overall capacitance (area enclosed by the voltammograms) compared to HKL-derived LCNFs. S190-SKL shows a much lower capacitance than S250-SKL. However, it keeps the rectangular shape of the voltammogram at higher rates, whereas S250-SKL shows a dramatic drop of its capacitance measured at a low scan rate. This correlates well with the difference in pore size distributions of both samples. S190-SKL consists of both (sub-)nanoporosity and mesopores as no crosslinking reactions took place, S250-SKL underwent crosslinking reactions and hence has a much narrower pore size distribution. Porous materials with pore sizes in a narrow range are less accessible by the ions in the electrolyte and thus give rise to low rate capabilities as observed here.

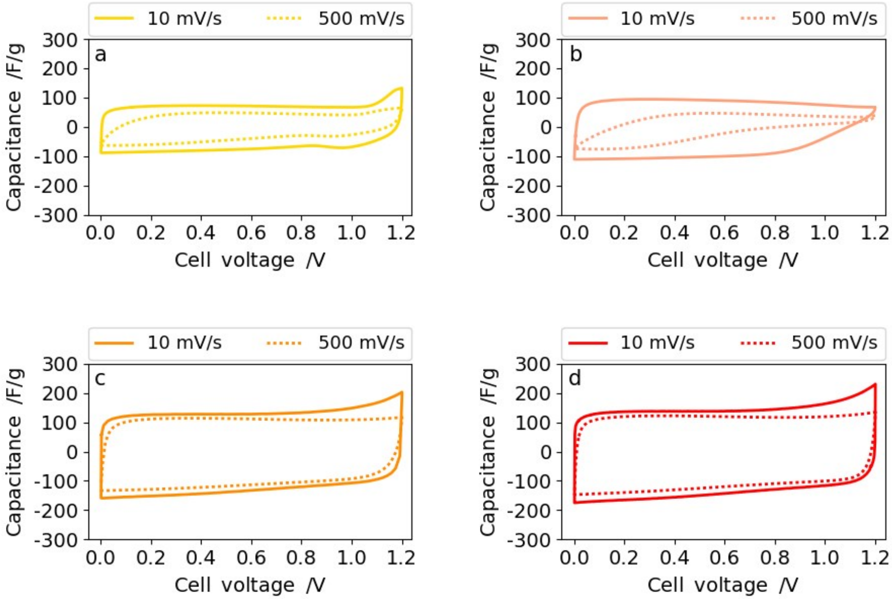

Figure S. 11 Cyclic voltammograms of S190-SKL (a), S250-SKL (b), S310-SKL (c), S340-SKL (d) at 10 and 500 mV/s.

Upon stabilization at higher temperatures (310 and 340 °C), a more open pore structure was created by both crosslinking and degradation reactions analogously to HKL. This gives rise to a leap in both overall capacitance and rate capability of the SKL-derived LCNFs (Figure S. 11).

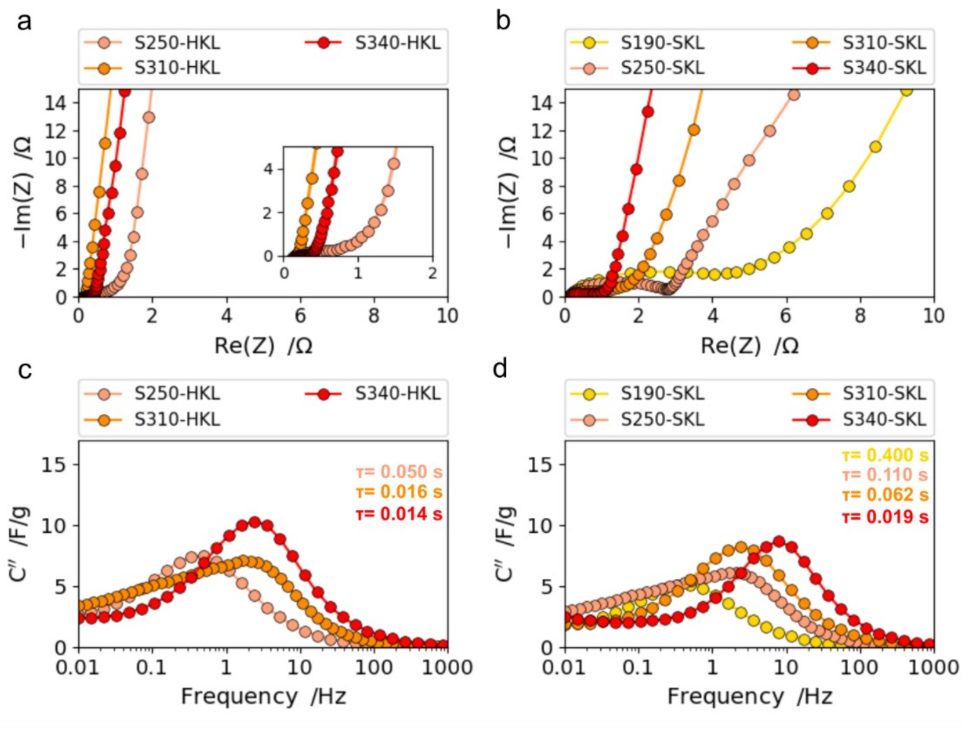

Figure S. 12 Nyquist plots of LCNFs derived from HKL (a) and SKL (b) and imaginary capacitance versus frequency plots for LCNFs derived from HKL (c) and SKL (d).

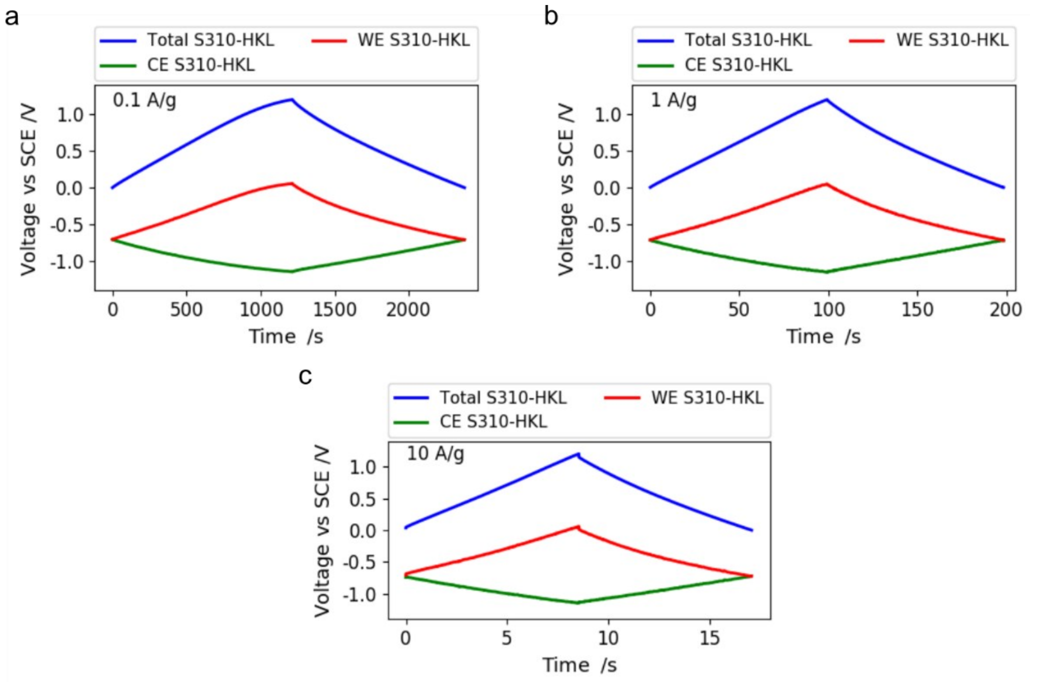

Figure S. 13 GCD profiles of S310-HKL measured in a three-electrode set-up at 0.1 (a), 1 (b) and 10 A/g (c). The working electrode profiles are shown in red, the counter electrode in green and the overall voltammogram in blue.

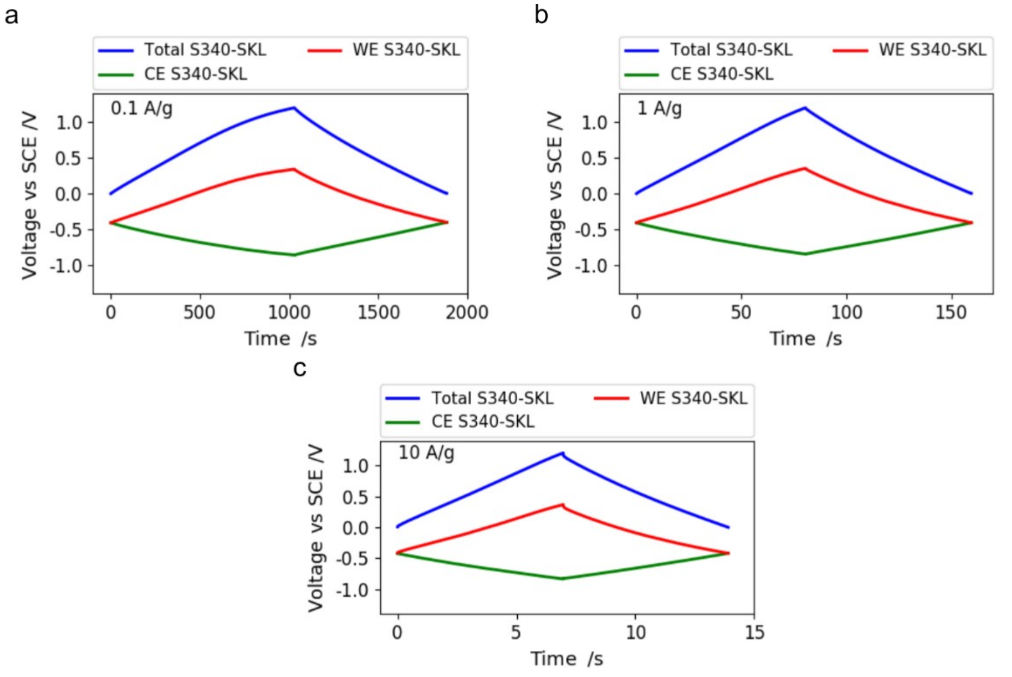

Figure S. 14 GCD profiles of S340-SKL measured in a three-electrode set-up at 0.1 (a), 1 (b) and 10 A/g (c). The working electrode profiles are shown in red, the counter electrode in green and the overall voltammogram in blue.

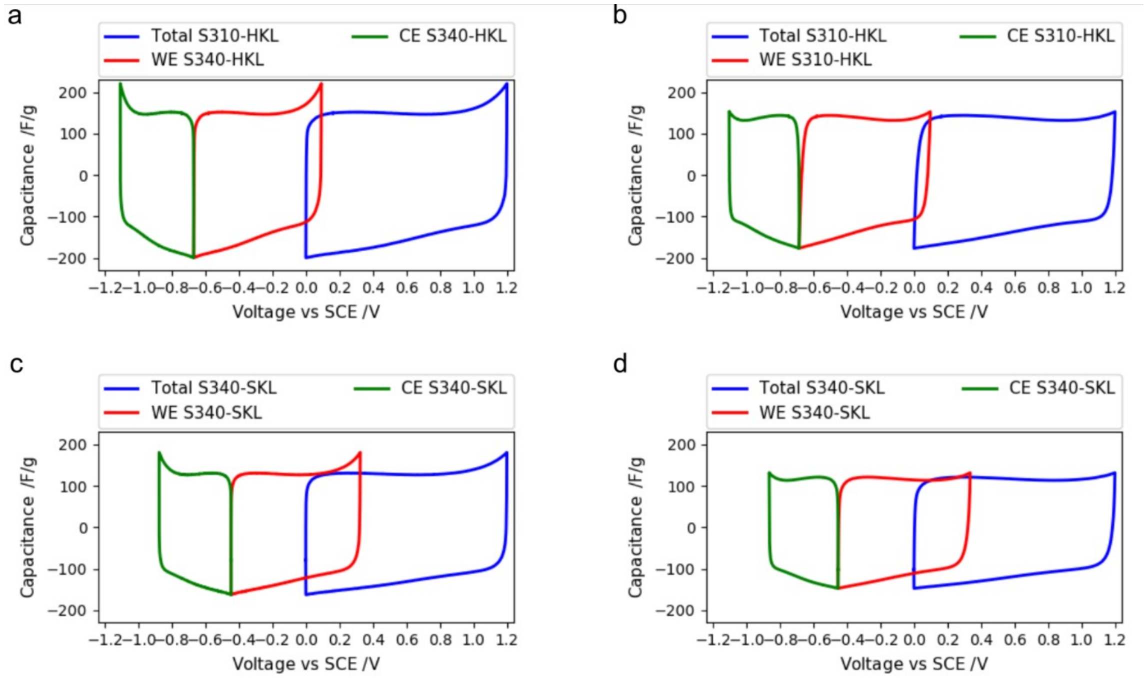

Figure S. 15 Cyclic voltammograms of S310-HKL (a and b) and S340-SKL (c and d) at 10 and 100 mV/s. The working electrode voltammograms are shown in red, the counter electrode in green and the overall voltammogram in blue.

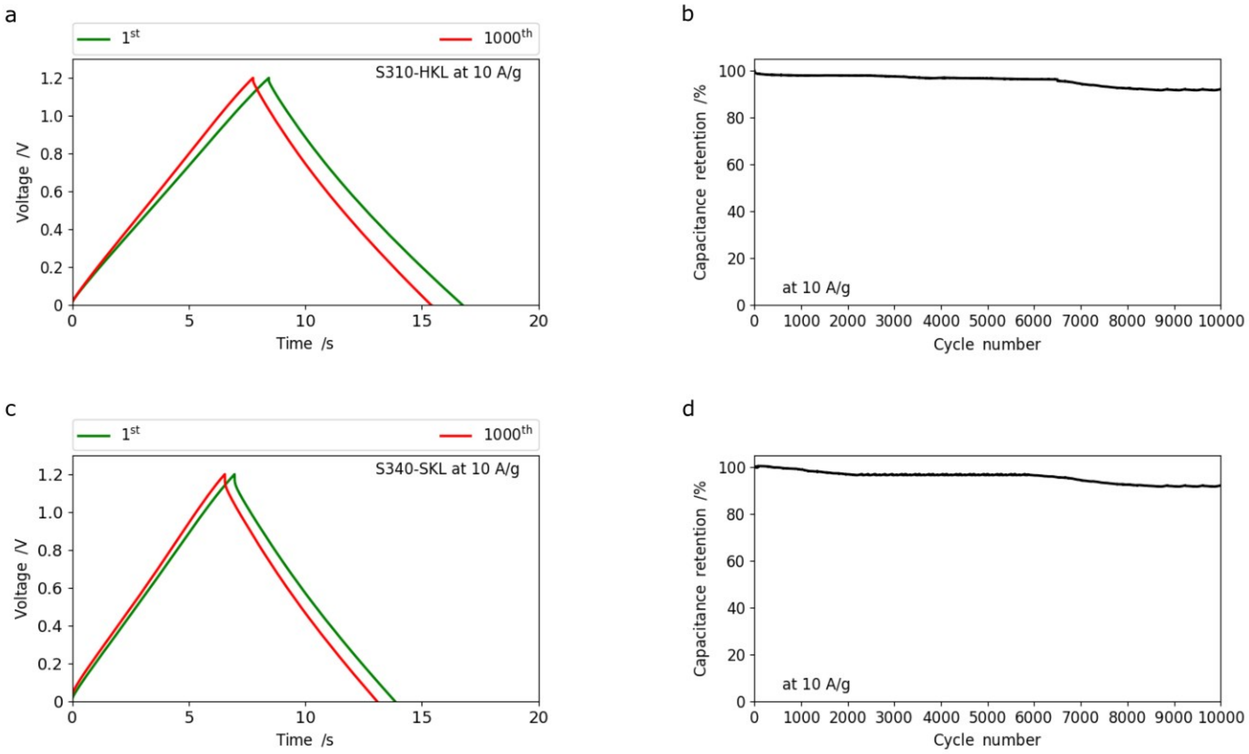

Figure S. 16 GCD profiles of S310-HKL at the 1st and the 10000th cycle (a), capacitance retention during 10000 charge-discharge cycles of S310-HKL (b), GCD profiles of S340-SKL at the 1st and the 10000th cycle (c), capacitance retention during 10000 charge-discharge cycles of S340-SKL (d).

1 C. M. Popescu, C. Vasile, M. C. Popescu, G. Singurel, V. I. Popa and B. S. Munteanu, *Cellul. Chem. Technol.*, 2006, **40**, 597–621.

2 C. G. Boeriu, D. Bravo, R. J. A. Gosselink and J. E. G. van Dam, *Ind. Crops Prod.*, 2004, **20**, 205–218.

3 C. S. Lancefield, S. Constant, P. de Peinder and P. C. A. Bruijnincx, *ChemSusChem*, 2019, **12**, 1114.

4 A. C. Ferrari and D. M. Basko, *Nat. Nanotechnol.*, 2013, **8**, 235–246.

5 M. Cho, F. K. Ko and S. Renneckar, *ACS Omega*, 2019, **3**, 5345–5355.